Human impacts on open ocean mercury concentrations

Elsie M. Sunderland[1] and Robert P. Mason[2]

Received 2 November 2006; revised 28 June 2007; accepted 30 August 2007; published 27 December 2007.

[1] We develop an empirically constrained multicompartment box model for mercury cycling in open ocean regions to investigate changes in concentrations resulting from anthropogenic perturbations of the global mercury cycle. Using Monte Carlo simulations, we explicitly consider the effects of variability in measured parameters on modeled seawater concentrations. Our simulations show that anthropogenic enrichment in all surface (25%) and deep ocean waters (11%) is lower than global atmospheric enrichment (300–500%) and varies considerably among geographic regions, ranging from >60% in parts of the Atlantic and Mediterranean to <1% in the deep Pacific. Model results indicate that open ocean mercury concentrations do not rapidly equilibrate with atmospheric deposition and on average will increase if anthropogenic emissions remain at their present level. We estimate the temporal lag between changes in atmospheric deposition and ocean mercury concentrations will vary from decades in most of the Atlantic up to centuries in parts of the Pacific.

Citation: Sunderland, E. M., and R. P. Mason (2007), Human impacts on open ocean mercury concentrations, *Global Biogeochem. Cycles*, *21*, GB4022, doi:10.1029/2006GB002876.

1. Introduction

[2] Methylmercury exposure causes many adverse health effects in humans and wildlife [*Champoux et al.*, 2006; *Clarkson and Magos*, 2006]. Marine fish and shellfish account for >90% of population-wide mercury intake in the United States and many of the largest exposure sources, such as tuna and swordfish, are harvested globally before being sold in domestic markets [*Sunderland*, 2007]. Anticipating changes in human exposure therefore relies on insight into spatial and temporal mercury trends in marine systems. Globally, the annual mercury release from ocean surface waters via gas exchange is approximately equivalent in magnitude to anthropogenic sources [*Mason and Sheu*, 2002; *Strode et al.*, 2007]. Hence understanding oceanic mercury cycling is also critical for accurately modeling deposition to terrestrial ecosystems. Here we develop an empirically constrained multicompartment box model for mercury cycling in open ocean regions to investigate changes in concentrations resulting from anthropogenic perturbations of the global mercury cycle.

[3] Many studies have shown differences in mercury concentrations among ocean basins [*Laurier et al.*, 2004; *Mason and Gill*, 2005]. For example, on average the Atlantic Ocean [*Dalziel*, 1995; *Mason et al.*, 1998a; *Mason and Sullivan*, 1999] appears to be enriched in mercury relative to the Pacific Ocean [*Gill and Fitzgerald*, 1988; *Laurier et al.*, 2004; *Mason and Fitzgerald*, 1991, 1993] but lower in concentration than the Mediterranean Sea [*Cossa et al.*, 1997, 2004]. Although several global-scale models for mercury cycling in ocean surface waters are available [*Lamborg et al.*, 2002; *Mason et al.*, 1994a; *Mason and Sheu*, 2002; *Strode et al.*, 2007], this modeling effort is the first to explicitly consider lateral mercury transport through ocean circulation and resulting spatial differences in mercury concentrations.

[4] Previous mercury cycling models assumed that ocean water achieves a rapid equilibrium with atmospheric inputs [*Lamborg et al.*, 2002; *Mason et al.*, 1994a; *Strode et al.*, 2007]. This assumption is inherent in all modeling frameworks that consider only a shallow (~100 m) surface layer interacting with the atmosphere. Such models effectively provide an upper bound for the temporal response of the ocean to changes in atmospheric deposition. By doing this, these models neglect the timescales associated with mixing of intermediate and deep waters with the surface layer of the ocean and do not consider the temporal changes in seawater concentrations most relevant for exposure of marine organisms to methylmercury. Other studies have suggested that the true mixed layer is greater than 100 m in many regions, especially those that experience seasonal deep water mixing, and that lateral transport is likely to affect surface water mercury concentrations and ocean response times. For example, *Laurier et al.* [2004] observed a shallow mixed layer with elevated mercury concentrations at the water surface (presumably due to atmospheric deposition) during summer months in the Pacific that disappeared during the winter months when mixed with deeper waters. In addition, data compiled by *Mason et al.* [1994b] suggest upwelling of thermocline waters in the equatorial Pacific is approximately equivalent to atmospheric inputs as a mercury source to surface waters and that mercury evasion in this region in

[1] U.S. Environmental Protection Agency, Office of Research and Development, Boston, Massachusetts, USA.
[2] University of Connecticut, Department of Marine Sciences, Groton, Connecticut, USA.

0886-6236/07/2006GB002876$12.00

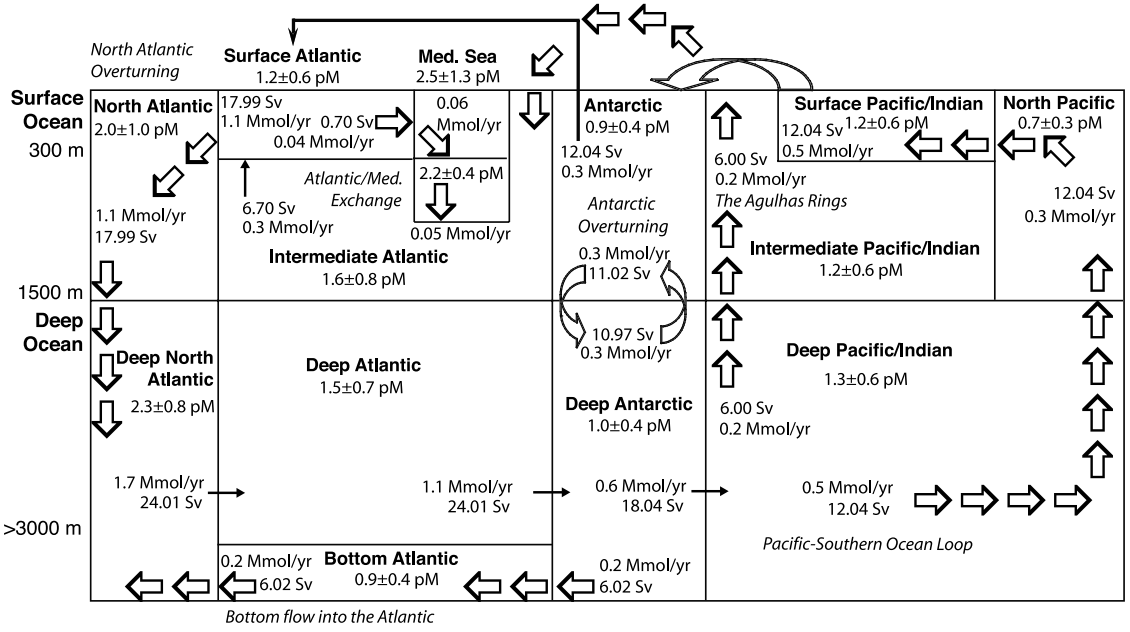

Figure 1. Overview of 14 compartment model adapted from *Kahana et al.* [2004] showing major ocean currents (block arrows) and steady state flows (smaller arrows) (1 Sv = 10^6 m^3 s^{-1}). Also shown are average present-day mercury concentrations (mean ± standard deviation) for each compartment and mercury fluxes resulting from seawater flow (Mmol a^{-1}). Note that sizes of model compartments are not to scale.

some cases exceeds atmospheric deposition. Because of this cycling, the authors hypothesized that upwelling waters in the Pacific, and likely other ocean regions, contain mercury deposited to surface waters up to a decade earlier that has been transported from higher latitudes. Similarly, *Cossa et al.* [2004] postulated that observed mercury-enriched subsurface waters from the northeast Atlantic Ocean (>5 pM) on the European continental margin represent a signal of historically deposited anthropogenic mercury transported by sinking water masses.

[5] In this study, we go beyond previous global mercury modeling efforts by incorporating linked surface and deep water compartments for different ocean basins that are affected by both lateral and vertical flow. Mixing layers for surface ocean compartments are based on the depths of the permanent thermocline, as specified by *Kahana et al.* [2004]. This framework allows us to investigate the longer timescales of mercury cycling and regional trends in mercury concentrations. Using a series of Monte Carlo simulations, we explicitly model the effects of variability in measured mercury concentrations used to parameterize the model on predicted seawater concentrations. We use existing global models for freshwater discharges, primary productivity, and carbon cycling to model mercury inputs from rivers and fluxes associated with sinking particulates in the water column. We apply the model to investigate how differences in predicted deposition rates from two global atmospheric fate and transport models (GEOS-Chem and GRAHM), which represent the latest understanding of atmospheric mercury chemistry [*Dastoor and Larocque*, 2004; *Selin et al.*, 2007a; *Selin et al.*, 2007b], and a simple empirical best estimate of basin-wide mercury loading affect near term trends in ocean mercury levels.

[6] We estimate the responsiveness of different ocean basins by running the empirically calibrated model in time-dependent mode to steady state with present-day atmospheric inputs. We also construct a preindustrial ocean mass budget using the physical rate constants derived from contemporary flux estimates and by assuming seawater concentrations were at steady state with the atmosphere prior to human influence. Comparing preindustrial and contemporary mercury budgets for each ocean basin allows us to calculate the cumulative anthropogenic enrichment of surface and deep ocean waters. This analysis provides a starting point for evaluating anthropogenic influences on past and future mercury exposure of pelagic marine organisms.

2. Model Description

2.1. General Model Description

[7] Here we present a global-scale model for mercury cycling in the oceans using a series of 14-linked boxes describing different ocean basins (Figure 1). We adapted the physical framework from a 16-compartment oceanographic model that is an expanded version of *Stommel*'s [1961] pioneering box model [*Kahana et al.*, 2004]. Because of a lack of mercury data for the Antarctic Ocean, we condensed

Table 1. Contemporary Surface Ocean Model Parameters

Latitude/Ocean Basin	Depth, m[a]	V_w, 10^{16} m^3	A_w, 10^{13} m^2	Q_r, 10^{12} L a^{-1}	$C_{ss}Q_r$, 10^{12} g a^{-1}	$C_{Hg(p)}$, nmol g^{-1}	$C_{Hg(d)}$, pM	k_w, m d^{-1}	$f_{Hg(0)}$, %	PP, Gt C a^{-1}
North Atlantic (>55°N)	1500	2.94	1.96	4415	670	0.4±0.2	3±2	0.16	24±16	0.98
Surface Atlantic (35°S–55°N)	300	1.85	6.16	17345	4164	1.0±0.5	15±10	0.57	13±09	7.07
Intermediate Atlantic (65°S–35°S)	1500	10.5	2.04	946	147	1.0±0.5	15±10	0.57	6±4	2.25
Surface Mediterranean (30°N–35°N)	300	0.075	0.25	946	489	1.4±0.7	4.5±2.3	1.37	6±5	0.34
North Pacific (>30°N)	1500	4.11	2.7	6623	4885	1.0±0.5	10±5	1.61	9±4	2.64
Surface Pacific/Indian (40°S–30°N)	300	4.44	14.8	6938	6558	0.6±0.3	15±10	1.69	6±4	16.99
Intermediate Pacific/Indian (65°S–40°S)	1500	25.3	5.0	negligible	negligible	n/a	n/a	1.69	3±2	5.66
Surface Antarctic (>65°S)	1500	1.73	1.2	11	17	0.4±0.2	3±2	0.16	9±6	0.54

[a]Depths of model compartments from *Kahana et al.* [2004] for surface ocean and *Tomczak and Godfrey* [1994] for deep ocean compartments (not shown) based on the average depth of each ocean, including adjacent seas. V_w = volume of model compartments; A_w = water surface area of each ocean basin; Q_r = freshwater discharges from rivers into each ocean basin based on data from *Dai and Trenberth* [2002]; $C_{ss}Q_r$ = discharge of suspended solids from rivers into oceans estimated from the average suspended sediment loads of rivers from *Ludwig et al.* [1996]; $C_{Hg(P)}$ and $C_{Hg(d)}$ are the particulate and dissolved phase concentrations of Hg in rivers flowing into the ocean from sources listed below; k_w = empirically calibrated water-side mass transfer coefficients used to estimate evasion of Hg(0) from each basin; $F_{Hg(0)}$ = average fraction of Hg(0) relative to total Hg in seawater estimated from empirical data; PP = primary productivity of each ocean basin from *Antoine et al.* [1996]; n/a = not applicable. River Hg concentrations from the following sources: North Atlantic/Antarctic, *Coquery et al.* [1995]; Surface/Intermediate Atlantic, *Maurice-Bourgoin et al.* [2003] and *Quemerais et al.* [1999]; Mediterranean, *Cossa et al.* [1997]; Pacific/Indian, *Subramanian et al.* [2003], *Tariq et al.* [1996], and *Woitke et al.* [2003]; North Pacific, *Han et al.* [2004] and *Choe et al.* [2003].

the four original compartments into two boxes in this study. We selected the *Kahana et al.* [2004] physical framework because its spatial resolution approximately matches the availability of empirical data needed to constrain the mercury cycling model. The physical model was calibrated using data on ocean currents from a variety of studies [*Kahana et al.*, 2004, and references therein]. In their assessment of the model's strengths and weaknesses, *Kahana et al.* [2004] concluded that the model successfully reproduces most present-day circulation patterns, responds in a physically realistic way, and matches observed thermohaline circulation at a performance level comparable to many GCMs. Although smaller-scale processes such as seasonal stratification and winter mixing of surface waters to depth are not captured by the model, reducing the complexity of ocean circulation patterns allows us to probabilistically simulate variability in observational mercury data with improved computational efficiency.

[8] Generally, the model framework is divided into surface and deep ocean compartments for the Atlantic Ocean, the Pacific/Indian oceans, and the Mediterranean Sea (Figure 1). Each of the 14 compartments is considered well mixed with respect to temperature, salinity, particulate matter, and mercury concentrations. Surface ocean compartments have depths that vary between 300 m and 1500 m (Table 1). High-latitude regions of the North Atlantic Ocean (>55°N) and the Arctic Ocean are both included in the surface ocean compartment denoted "North Atlantic." Two intermediate ocean compartments underlie the Atlantic and Pacific/Indian oceans and also include regions that interact directly with the atmosphere (Figure 1). The deep ocean begins at 1500 m depth for most compartments (3900 m for the Bottom Atlantic) and extends to the average seafloor depth for each basin (Table 1 and Figure 1).

[9] The model can be run in either a deterministic or probabilistic mode using the general form of the relationships presented in equations (1)–(3). For each basin, we model time-dependent changes in the mercury reservoir (M, Mmol) in surface (M_S), intermediate (M_{Int}) and deep (M_D) water compartments using Euler-type numerical integration as follows:

$$\frac{dM_S}{dt} = Atm_s + R_s + \sum_i^n k_{oi}M_i - (k_v + k_{ws} + k_o)M_s \quad (1)$$

$$\frac{dM_{Int}}{dt} = Atm_{Int} + R_{Int} + \sum_i^n k_{oi}M_i + k_{ws}M_s(k_v + k_{ws} + k_o)M_{int} \quad (2)$$

$$\frac{dM_D}{dt} = \sum_i^n k_{oi}M_i + k_{ws}M_{Int}(k_o + k_{ws})M_D \quad (3)$$

where, Atm is atmospheric mercury deposition (Mmol a^{-1}); R is mercury loading from rivers (Mmol a^{-1}); k_o is the annually averaged rate constant (1 a^{-1}) for seawater outflow through deep water formation, upwelling and lateral flow or, conversely, k_{oi} is the rate constant for seawater inputs from the source basin, i; k_{ws} is the rate constant for settling of suspended particulate matter; and k_v is the rate constant for volatilization/gas exchange from surface and intermediate model compartments.

[10] Deep ocean compartments may also receive mercury inputs from hydrothermal vents and ocean floor sediments through diffusion and resuspension. We do not include these fluxes here because inputs from bottom sediments are expected to be insignificant relative to the total mercury reservoir in deep ocean waters [*Lamborg et al.*, 2002; *Mason et al.*, 1994a; *Mason and Sheu*, 2002] and *Lamborg et al.* [2006] recently estimated that hydrothermal sources are likely less than 0.1 Mmol a^{-1}.

[11] We develop both contemporary and preindustrial mass budgets for mercury in each ocean basin. The present-day mass budget is constrained by measured mercury concentrations and fluxes. We assume physical rate constants derived from contemporary flux measurements will be

Table 2. Observed Seawater Hg Data (Mean ± Standard Deviation) Reported in the Literature

Ocean Basin	Hg, pM	Hg(0), pM	Evasion Hg(0), nmol m^{-2} d^{-1}
North Atlantic	2.4±1.6[a] 1.57±0.44[b] 2.1±0.6[c]	0.41±0.31[a]	1.9±1.3[a] 0.156[d]
Deep North Atlantic	2.3±0.8[e]	n/a	n/a
South and equatorial Atlantic	1.68±0.74[f] 2.9±1.7[g]	1.2±0.8[f] 0.08–0.16[h] 0.11[i]	0.323[i] 9.6[j]
Deep Atlantic/Bottom Water	1.7±0.7[k] 0.96±0.41[l] 0.9±0.4[m]	n/a	n/a
Mediterranean	2.2±0.4[n] 2.54±1.25[o] 1.46±0.41[p]	0.15±0.12[p] 0.08–0.21[i,q]	0.14[r] 0.23–0.48[q] 0.28–0.94[i]
North Pacific	0.64±0.26[s]	0.06±0.03[r]	0.88±0.11[r]
South and equatorial Pacific	1–2[t,d]	0.13±0.07[r] 0.04–0.32[d] 0.06–0.14[u]	0.29±0.26[u] 0.40[d]
Deep Pacific/Indian	1.2±0.3[s]	n/a	n/a
Antarctic	0.7–1.1[v]	no data	no data

[a]Profile averages for samples taken between 50–70°N from *Mason et al.* [1998a].
[b]North Atlantic Surface Water flowing into the Mediterranean Sea measured by *Cossa et al.* [1997].
[c]European continental shelf margin from *Cossa et al.* [2004].
[d]*Mason and Fitzgerald* [1991, 1993].
[e]Water depths >1500 m, >50°N from *Mason et al.* [1998a].
[f]Subsurface water from the south and equatorial Atlantic from *Mason and Sullivan* [1999].
[g]Surface water samples from the south and equatorial Atlantic from *Mason and Sullivan* [1999].
[h]*Mason et al.* [2001].
[i]*Gardfeldt et al.* [2003].
[j]*Lamborg et al.* [1999].
[k]Seawater below 1500 m in the Deep Atlantic from *Mason and Sullivan* [1999].
[l]Below 1500 m average from *Dalziel* [1995].
[m]Below 3300 m from *Dalziel* [1995].
[n]Seawater exiting the Strait of Gibraltar from *Cossa et al.* [1997].
[o]Also in the western Mediterranean.
[p]*Horvat et al.* [2003].
[q]*Ferrara et al.* [2003].
[r]*Laurier et al.* [2003].
[s]*Laurier et al.* [2004].
[t]*Gill and Fitzgerald* [1988].
[u]*Dalziel* [1995], *Laurier et al.* [2004], and *Mason and Sullivan* [1999] detected Antarctic Bottom Water and Antarctic Intermediate Waters in the Atlantic and Pacific oceans.
[v]*Kim and Fitzgerald* [1986].

comparable in both models and the preindustrial ocean is at steady state with preindustrial atmospheric and freshwater mercury inputs estimated from historic data.

2.2. Reservoirs of Mercury in Surface and Deep Ocean Compartments

[12] We calculate present-day ocean mercury reservoirs from the volume of each basin and previously measured seawater mercury concentrations shown in Table 2. For probabilistic simulations, we fit lognormal distributions to the available mercury concentration data for each ocean basin. Overall, we specify a contemporary global mean of 1.3 ± 0.4 pM, which is comparable to the range of 1.5–2.0 pM estimated in other studies [*Lamborg et al.*, 2002; *Mason et al.*, 1994a; *Mason and Sheu*, 2002; *Strode et al.*, 2007]. The estimated reservoir of mercury in the surface ocean is substantially higher in this study (average: 670 Mmol, 90% confidence intervals: 470–900 Mmol) relative to previous work (53–500 Mmol) because our mixed layer (based on the depth of the permanent thermocline) ranges between 300–1500 m, compared to 53–500 m in other studies [*Lamborg et al.*, 2002; *Mason et al.*, 1994a; *Mason and Sheu*, 2002; *Strode et al.*, 2007].

2.3. Atmospheric Deposition

[13] Contemporary atmospheric mercury deposition over each ocean basin is modeled using two global 3-D atmospheric chemistry transport models (GEOS-Chem and GRAHM) and a simple empirically based algorithm. GEOS-Chem outputs are based on model version 7.04 (http://www.as.harvard.edu/chemistry/trop/geos/) using meteorological data for the years 2000–2005 and global anthropogenic emissions in 2000, described in detail by *Selin et al.* [2007a]. GEOS-Chem uses assimilated meteorological data from the NASA Goddard Earth Observing Systems (GEOS-4), including winds, mixed layer depths, temperature, precipitation, and convective mass fluxes. Results for elemental mercury (Hg(0)), divalent mercury (Hg(II)), and particulate mercury (Hg(P)) deposition are produced by GEOS-Chem at the 4° × 5° horizontal resolution and summed over the surface area corresponding to each surface ocean compartment in our model. We only consider deposition of Hg(II) and Hg(P) in this study because bidirectional Hg(0) exchange is accounted for by the net evasion term in the ocean model.

[14] Similarly, GRAHM (Global/Regional Atmospheric Heavy Metals Model) deposition rates are based on anthropogenic emissions for the year 2000 [*Pacyna et al.*, 2006; *Wilson et al.*, 2006] and meteorological data for 2001 from Canada's Global Environmental Multiscale (GEM) model [*Dastoor and Larocque*, 2004]. GRAHM model results presented by *Dastoor and Larocque* [2004] do not include natural and recycled releases of mercury from land and oceans that are included in the model version applied in this study (A. Dastoor, personal communication, 2006). We sum modeled deposition for Hg(P) and Hg(II) predicted at the 1° × 1° horizontal resolution over the surface area of each ocean basin in the box model.

[15] Empirically estimated atmospheric deposition rates are based on previous modeling efforts [*Mason and Sheu*, 2002; *Mason and Gill*, 2005]. Here we constrain cumulative wet (Atm_{wet}) and dry (Atm_{dry}) deposition over the oceans using previous global mass budgets [*Mason and Sheu*, 2002]. We distribute cumulative deposition spatially as a function of observed reactive gaseous mercury concentrations (assumed to be equivalent to Hg(II)) (equation (4)), average rainfall (P), and observed atmospheric Hg(0) concentrations in the marine boundary layer (MBL) above each ocean compartment (equation (5)):

$$Atm_{dry} = a_d\left(C_{a(Hg(II))}v_d\right)A_w \tag{4}$$

$$Atm_{wet} = a_w\left(C_{a(Hg(0))}R_wP\right)A_w \tag{5}$$

[16] As shown in equation (4), we calculate dry deposition (Mmol a^{-1}) over each ocean basin as the product of observed reactive gaseous mercury in the MBL ($C_{a(Hg(II))}$, pg m^{-3}), an average deposition velocity (v_d, cm s^{-1}), and a conversion factor ($a_d = 1.58 \times 10^{-13}$ Mmol a^{-1}/pg s^{-1}). For simplicity, v_d is assumed to be 1 cm s^{-1} over all ocean basins [*Laurier et al.*, 2003; *Hedgecock and Pirrone*, 2004]. We calculate wet deposition (equation (5)) as the product of atmospheric Hg(0) concentrations ($C_{a(Hg0)}$, ng m^{-3}), a dimensionless empirically estimated exchange coefficient (R_w), mean annual rainfall (P, m a^{-1}), the surface area of each ocean basin interacting with the atmosphere (A_w, m^2), and a conversion factor ($a_w = 5 \times 10^{-18}$ Mmol ng^{-1}). The exchange coefficient, R_w, approximates the fraction of Hg(0) that is oxidized in the MBL and troposphere to Hg(II) and subsequently scavenged from the atmosphere into precipitation (as both gaseous and particulate Hg(II)). R_w is based on an empirically defined relationship between observed Hg(0) concentrations in the MBL and measured wet deposition of Hg(II) [*Mason et al.*, 1994a; *Mason and Sheu*, 2002]. Accordingly, our empirically estimated deposition mimics observed trends in MBL Hg(0) concentrations. Experimental data indicate there is a north-south gradient in MBL Hg(0), with concentrations being a factor of 2–3 greater in the Northern Hemisphere as well as higher concentrations over the Atlantic compared to the Pacific Ocean [*Lamborg et al.*, 1999; *Slemr et al.*, 2003; *Temme et al.*, 2003]. Although in the empirical model R_w is a simplified approximation of Hg(0) oxidation and Hg(II) scavenging in precipitation, this is not so for the GEOS-Chem and GRAHM models, which include a variety of chemical mechanisms for Hg(0) oxidation and deposition [*Dastoor and Larocque*, 2004; *Selin et al.*, 2007a]. Empirically estimated dry particulate deposition is assumed to be 1% of wet deposition on the basis of the results of other studies [*Lamborg et al.*, 1999; *Mason et al.*, 1994a].

[17] Global preindustrial atmospheric deposition is also constrained to estimates from previous studies [*Mason and Sheu*, 2002]. Using the algorithms described in equations (4) and (5) above, we model deposition over each ocean basin by assuming Hg(0) concentrations are globally uniform and the fraction of total gaseous mercury present as Hg(II) will not change between the present and contemporary simulation (i.e., $C_{aHg(II)}$ is estimated as a function of preindustrial $C_{aHg(0)}$). Uniform distributions of Hg(0) are plausible as a first approximation of the preindustrial atmosphere because present-day latitudinal gradients are thought to be mainly the result of regional differences in anthropogenic emissions [e.g., *Lamborg et al.*, 2002; *Slemr et al.*, 2003]. We estimate that preindustrial atmospheric Hg(0) concentrations are approximately 0.63 ng m^{-3}. This is consistent with the modeling efforts of *Dastoor and Larocque* [2004], which show that anthropogenic emissions contribute ~0.2 ng m^{-3} of the observed Hg(0) (~0.8 ng m^{-3}) in the Southern Hemisphere and ~0.45–0.6 ng m^{-3} in the Northern Hemisphere (~1.5–2.5 ng m^{-3}).

2.4. Freshwater Discharges

[18] We calculate mercury inputs from rivers (R, Mmol a^{-1}) using data on long-term mean freshwater discharges (Q_r) to each ocean basin and average sediment loads (C_{ss}, mg L^{-1}) for the largest 927 rivers globally [*Dai and Trenberth*, 2002; *Ludwig et al.*, 1996]. We compiled available dissolved ($C_{Hg(d)}$, pM) and particulate ($C_{Hg(p)}$, μmol mg^{-1}) phase mercury concentration data from major rivers (Table 1) and fit distributions to the observed ranges for the probabilistic model. We model mercury inputs to each surface ocean compartment using the following general relationship:

$$R = Q_r\left(10^{-18}C_{Hg(d)} + 10^{-12}C_{ss}C_{Hg(P)}\right) \tag{6}$$

[19] For some model compartments there were insufficient empirical data to characterize probability distributions for mercury concentrations. In these cases we assume data are lognormally distributed with confidence intervals of ±50% based on data reported by *Cossa et al.* [1997] for rivers flowing into the Mediterranean Sea.

[20] Other studies show most of the suspended particulate load in rivers deposits around the river mouth (~70%) and on the continental shelf (~20%) [*Chester*, 2003; *Cossa et al.*, 1997] and only ~10% reaches the open ocean. We therefore estimate mercury inputs from rivers to the open ocean as 10% of the particle associated discharges and all of the dissolved phase flow.

[21] For the preindustrial model, we constrain fluxes from rivers using concentration data from sediment cores. Globally, anthropogenic mercury enrichment in sediment cores in remote regions varies between 200–500% [*Fitzgerald et al.*, 1998; *Hermanson*, 1993] and is much greater in areas close to point sources of current or historic contamination [*Pirrone et al.*, 1998]. Extrapolating from these data, we divide present-day mercury concentrations in rivers by a factor of 5 to account for anthropogenic enrichment in terrestrial systems affected by effluent mercury releases, in addition to enhanced atmospheric deposition from anthropogenic emissions.

2.5. Rate Constants

2.5.1. Lateral Flow, Upwelling, and Deep Water Formation

[22] Rate constants (1 a^{-1}) for water outflow (k_o) from each model compartment are calculated from the total

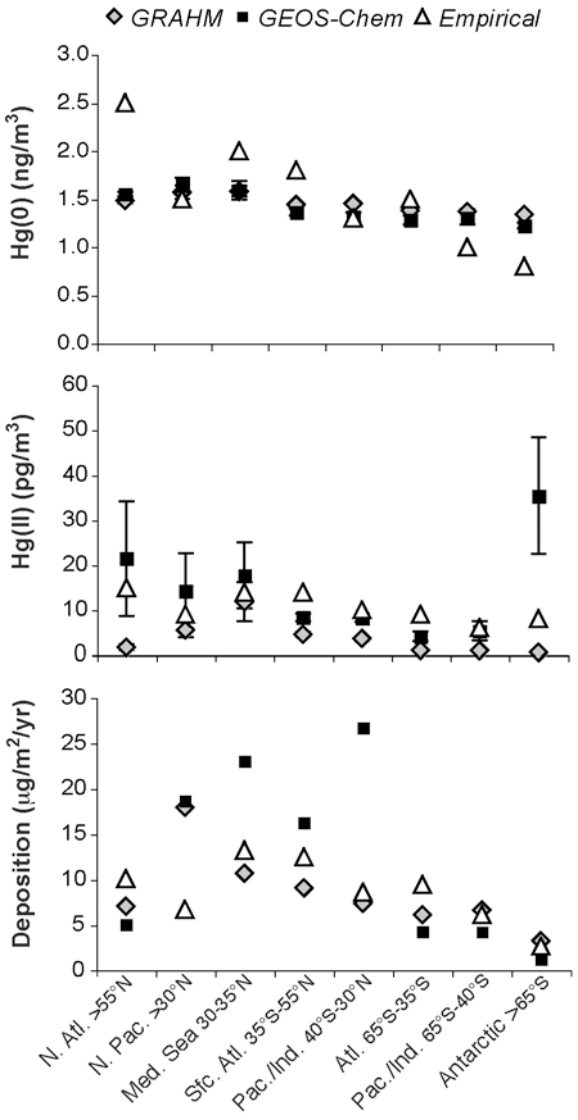

Figure 2. Summed results from three atmospheric models for each ocean basin. Results for Hg(0) and Hg(II) concentrations represent averages in 100 m layer above the surface of each basin.

outflow (F_o, m^3 a^{-1}) reported by *Kahana et al.* [2004] divided by the estimated volume of each compartment (V_w, m^3). That is:

$$k_o = F_o / V_w \tag{7}$$

[23] Mercury inflow to each ocean basin resulting from lateral water movements, upwelling, and deep water formation is modeled as the product of the rate constant for water outflow from the contributing basin and the mercury reservoir in that basin.

2.5.2. Gas Exchange

[24] We assume that the rate constants (k_v) for loss of Hg(0) from seawater can be reasonably approximated from available data on present-day fluxes (F_v, Mmol a^{-1}) and the total mercury reservoir in each basin. Here we use a simplified representation of the two-layer thin film transfer model [*Liss and Slater*, 1974] (equation (8)) to estimate an annually averaged evasion rate constant for Hg(0) loss from each ocean basin (equation (9)):

$$F_v = k_w \left(f_{Hg(0)} C_w\right) 10^{-15} A_w \tag{8}$$

$$k_v = \frac{k_w \left(f_{Hg(0)}\right) 10^{-15} A_w}{V_w} \tag{9}$$

where k_w (m d^{-1}) is the annually averaged water-side mass transfer coefficient for each basin, $f_{Hg(0)}$ is the fraction of mercury present as Hg(0) in seawater, C_w (pM) is the total mercury concentration in seawater, and 10^{-15} is the appropriate units conversion factor.

[25] In the simplified model, we neglect terms for atmospheric Hg(0) concentrations and the air-side mass transfer coefficient because Hg(0) is generally supersaturated in the water column [e.g., *Andersson et al.*, 2007; *Mason et al.*, 1998a] and basin-wide average atmospheric Hg(0) is small (1.0–2.5 fM; Figure 2) compared water column concentrations (63–480 fM) (Tables 1 and 2). Much of the empirical data (Table 2) on Hg(0) concentrations and estimated fluxes appears to be biased high because estimated losses could not be sustained on an annual basis without depleting observed surface ocean concentrations or increasing observed atmospheric Hg(0) levels [*Gardfeldt et al.*, 2003; *Lamborg et al.*, 1999; *Mason et al.*, 1998a, 2001]. This bias may be the result of sampling during summer months when there is potentially enhanced biological and photochemical production of Hg(0) [*Mason et al.*, 1995a, 1995b, 1998a] that is greater than effects of increased wind speed in the winter [*Strode et al.*, 2007], or may reflect large bidirectional exchange of Hg(0) in the marine boundary layer [*Mason and Sheu*, 2002; *Selin et al.*, 2007b]. Given these uncertainties in measured fluxes, we constrain average total evasion from the oceans to previous global estimates [*Mason and Sheu*, 2002]. We calibrate regional basin-wide water-side mass transfer coefficients (k_w) using low estimates of both measured fluxes and the fraction of Hg(0) ($f_{Hg(0)}$) in seawater (Table 2) to account for this high bias. These empirically calibrated mass transfer coefficients capture regional differences in annual evasion rates resulting from variability in average wind speeds [*Nightingale et al.*, 2000] as well as other processes. Where data are available, we fit lognormal distributions to measured $f_{Hg(0)}$ data (Table 2) and assume the same $f_{Hg(0)}$ ranges to proximal basins at similar latitudes for systems with no data. For the preindustrial model, we calculate evasion as a function of the reservoir of mercury in each preindustrial ocean basin and the empirically calibrated k_v and $f_{Hg(0)}$ described above.

2.5.3. Particulate Settling

[26] We model contemporary mercury fluxes associated with suspended particulate matter fluxes as a function of primary productivity (PP) and carbon attenuation in each ocean basin using the mercury to carbon ratio (0.6 ng Hg/mg C) estimated by *Mason et al.* [1994a]. For the proba-

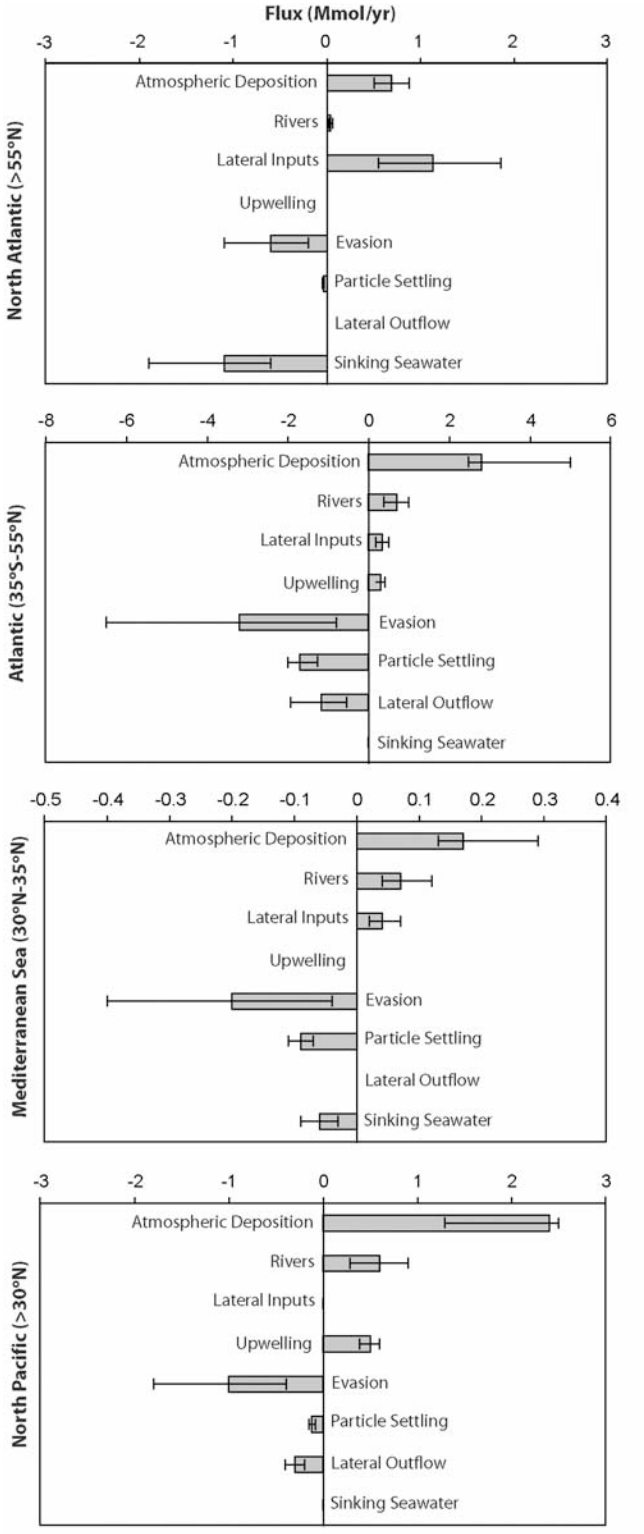

Figure 3. Fluxes of mercury (Mmol a^{-1}) for selected ocean basin. Error bars represent variability among models for atmospheric deposition and 90% confidence intervals for all other fluxes.

bilistic simulation we sample mercury to carbon ratios from a uniform distribution (no data are available to characterize this distribution) around this mean value with a standard deviation of ±20% on the basis of studies showing mercury concentrations commonly vary by this amount [e.g., *Mason et al.*, 1998b]. Global productivity (36.5 Gt C a^{-1}) and PP estimates for each ocean basin are taken from *Antoine et al.* [1996] (Table 1), while carbon flux is modeled using the relationship developed by *Antia et al.* [2001]:

$$J_{orgC} = 0.1 PP^{1.77} z^{n} \quad (10)$$

where J_{orgC} (g C m^{-2} a^{-1}) is the flux of organic carbon, PP (g C m^{-2} a^{-1}) is total primary productivity in each model compartment, z (m) is the effective depth for which the particulate flux is calculated, and n is the exponent describing the relationship between declines in organic carbon flux due to mineralization in the water column with depth. For the Pacific Ocean, $n = -0.74$ [*Pace et al.*, 1987], and for all other compartments we assumed $n = -0.68$ on the basis of measurements in the Atlantic Ocean [*Antia et al.*, 2001]. We do not include temperature dependence in our model because we are primarily interested in fluxes at depths of 1500 m and greater (minimum 300 m). Other studies suggest effects of temperature on carbon attenuation are most pronounced in the upper 125 m of the water column and that variability is small in deeper ocean waters [*Antia et al.*, 2001; *Howard et al.*, 2006; *Laws et al.*, 2000]. Our modeled total organic carbon fluxes in intermediate and deep waters of the Atlantic at 1500 m (0.25 Gt C a^{-1}) and at 3300 m (0.14 Gt C a^{-1}) compare favorably to fluxes for the entire Atlantic Ocean estimated by *Jahnke* [1996] at 1000 m (0.39 Gt C a^{-1}) and at the seafloor (0.14 Gt C a^{-1}).

[27] Empirically derived rate constants for particle settling (k_{ws}, 1 a^{-1}) are based on the contemporary settling flux and the mercury reservoir in each compartment. For the preindustrial model, mercury to carbon ratios are calibrated to match deep ocean burial reported by *Mason and Sheu* [2002], resulting in a three-fold reduction in mercury concentrations. This reduction agrees well with the estimated range of anthropogenic mercury enrichment in remote regions [*Fitzgerald et al.*, 1998]. We did not directly link preindustrial mercury to carbon ratios (used to derive rate constants for particulate settling) to water column mercury concentrations. No data were available to quantify the influence of inputs from terrestrial systems on regional variability in particulate fluxes, and thus an empirical mercury to carbon ratio was chosen for the simulations. However, the mercury flux associated with particle settling will depend on the composition and concentrations of abiotic and biotic matter in suspended solids in the water column.

2.6. Uncertainty and Sensitivity Analysis

[28] Monte Carlo simulations (100,000 trials for each scenario explored) were used to quantify the effects of measurement errors, underdetermined model parameters, and natural stochasticity in mercury concentrations used to constrain the ocean model. Parameters sampled probabilistically by the model include total mercury in seawater, dissolved and particulate phase mercury in freshwater dis-

charges, the fraction of mercury present as Hg(0) in the water column, and mercury to carbon ratios of suspended particulate matter. Measured mercury concentrations and fluxes described in each of the preceding sections were used to fit distributions sampled during Monte Carlo trials.

[29] For mass budgets, 90% confidence limits were calculated from variability in mercury data discussed above. In addition, we determine expected seawater concentrations and relative enrichment estimates from the summed product of forecasted seawater concentrations and their probabilities of occurrence. We also analyzed sensitivity of results to variability in mercury concentrations used to parameterize the model. We report ranked contributions of each uncertain term as percentages of total variance in model results.

3. Model Results and Discussion

3.1. Regional Fluxes

[30] Table 3 shows a summary of empirically constrained contemporary mercury reservoirs and fluxes in each ocean basin. Atmospheric deposition generally dominates mercury inputs to surface ocean waters (Figure 3 and Table 3). On a global scale, simulated present-day atmospheric deposition to the oceans ranges between 14 Mmol a^{-1} and 29 Mmol a^{-1} among the three models. Differences among models are, in part, a function of the amount of the global Hg(0) pool deposited over land relative to water in GEOS-Chem framework as described by *Selin et al.* [2007b]. Comparing results on a regional basis indicates that most of the difference is due to enhanced GEOS-Chem deposition over the Pacific/Indian oceans between 40°S and 30°N (19.8 Mmol a^{-1}) relative to the empirical (6.4 Mmol a^{-1}) and GRAHM (5.4 Mmol a^{-1}) models. Average mercury deposition rates (Figure 2) from GEOS-Chem over the Mediterranean Sea (23 μg m^{-2} a^{-1}) and Atlantic Ocean between 35°S–55°N (16 μg m^{-2} a^{-1}) are also notably higher than the other two models (11–13 μg m^{-2} a^{-1} and 9–12 μg m^{-2} a^{-1}, respectively). It appears that the mechanistic atmospheric fate and transport models currently have difficulty capturing observed increases in Hg(0) and reactive gaseous mercury (Hg(II)) in northern regions (Figure 2), particularly the high concentrations observed over the Atlantic Ocean [*Lamborg et al.*, 1999; *Slemr et al.*, 2003; *Temme et al.*, 2003]. However, the strengths and weaknesses of different modeling results remains equivocal until additional empirical data are available to evaluate performance. Details of formulation and assumptions in the GEOS-Chem and GRAHM models can be found elsewhere [*Dastoor and Larocque*, 2004; *Selin et al.*, 2007a, 2007b] and are beyond the scope of this study.

[31] When compared to atmospheric deposition, other mercury fluxes for lateral and vertical seawater flow, particulate settling, and evasion vary substantially in relative importance across different geographic regions (Table 3). Our results show lateral and vertical mercury flows are greater in magnitude than atmospheric deposition in the North Atlantic (>55°N) (Figure 3) and are the main source of mercury transport in deep ocean waters (Table 3). Although on a global scale, rivers are often neglected as sources of mercury to open ocean regions [*Lamborg et al.*, 2002; *Strode et al.*, 2007], here we show that fluxes from rivers can be important on a regional basis. For example, inputs from rivers are between 25% and 41% of atmospheric deposition in the Surface Atlantic (35°S–55°N), North Pacific (>30°N) and Mediterranean Sea but are negligible in the North Atlantic and the rest of the Pacific (Table 3 and Figure 3). Similarly, particle associated losses of mercury are >60% of the magnitude of atmospheric inputs and comparable to evasion as a loss mechanism in shallow surface waters of the Atlantic (35°S–55°N) (Figure 3). At higher latitudes and in deeper waters particle-associated fluxes are much smaller than atmospheric inputs and lateral seawater flow (Table 3 and Figure 3). Evasion of mercury at the air-water interface is the dominant loss mechanism in most surface ocean basins (Figure 3). Both the surface Atlantic Ocean (35°S–55°N) and Mediterranean Sea appear to be net sources of mercury to the atmosphere, although 90% confidence intervals for evasion estimates are wide because of a paucity of empirical data. Our results for the Mediterranean Sea showing annual evasion rates between 40–400 kMol (mean 200 kMol) and atmospheric deposition between 130–290 kMol (midrange 170 kMol) agree with recent field measurements and modeling efforts that predict net atmospheric losses to be ~40 kMol a^{-1} [*Rajar et al.*, 2007; *Zagar et al.*, 2007]. These regional differences in physical and biological factors affecting mercury cycling help explain why seawater concentrations vary among ocean regions. In contrast, many previous studies have conjectured that changes in atmospheric loading will result in proportional near-term differences in marine fish mercury concentrations, thereby assuming atmospheric sources are the only determinant of seawater mercury concentrations and biological exposure [e.g., *Rice and Hammitt*, 2005; *Trasande et al.*, 2005].

3.2. Contemporary Global Mass Budget

[32] Our contemporary global mass budget is based on empirically constrained mercury exchanges between surface and deep ocean compartments. To avoid double counting of vertical flows and settling fluxes when aggregating regional modeling results with different mixing depths, in Figure 4 we only show flow and fluxes of mercury across the 1500 m surface layer and the deep ocean. Sinking of surface waters in the Mediterranean Sea and upwelling from the Intermediate Atlantic to the Surface Atlantic model compartments (Figure 1) are not included in this illustration of the global budget but are included computationally in all regional-scale modeling. Internal advective transport within surface (1.3–4.0 Mmol a^{-1}, mean 2.5) and deep waters (2.3–5.8 Mmol a^{-1}, mean 3.9) is greater than vertical flows (means 1.0 and 1.4 Mmol a^{-1}) but not shown in Figure 4 because lateral flow does not result in any net transport between the surface and deep ocean layers. Similarly, particle associated fluxes of mercury across the 1500 m depth shown in Figure 4 are small (2.2 Mmol a^{-1}), relative to modeled fluxes at 300 m depth across the entire surface ocean (~6.9 Mmol a^{-1} based on equation (10) above). These results highlight the importance of using both regional modeling and global mass budgets to better understand mercury dynamics in surface and deep ocean waters.

[33] Overall, our global mass budget indicates that the ocean is not presently at steady state with atmospheric inputs.

Table 3. Contemporary Ocean Reservoirs and Fluxes in (+) and out (−) of Each Compartment Shown as Means and 90% Confidence Limits[a]

Basin	Reservoir	Atmospheric Deposition			Evasion	Particulate Settling	Rivers	Lateral Flow	Vertical Flow
		GC	GH	EM					
North Atlantic	59 (29–96)	0.50	0.69	0.88	−0.6 (0.2–1.1)	−0.04 (0.03–0.05)	+0.04 (0.02–0.06)	+1.1 (0.6–1.9)	−1.1 (0.6–1.9)
Surface Atlantic	37 (18–61)	5.0	2.8	2.5	−3.2 (0.8–6.5)	−1.7 (1.3–2.0)	+0.7 (0.4–1.0)	+0.3 (0.2–0.5) −1.2 (0.6–1.9)	+0.3 (0.2–0.4)
Intermediate Atlantic	167 (82–274)	0.44	0.62	1.2	−0.4 (0.1–0.8)	+1.7 (1.3–2.0) −0.7 (0.6–0.9)	+0.03 (0.02–0.04)	+0.3 (0.1–0.5)	−0.3 (0.2–0.4)
Surface Mediterranean	2 (1–3)	0.29	0.13	0.17	−0.2 (0.04–0.4)	−0.09 (0.07–0.1)	+0.07 (0.04–0.1)	+0.04 (0.02–0.07)	−0.06 (0.03–0.09)
North Pacific	29 (17–43)	2.5	2.4	1.3	−1.0 (0.4–1.8)	−0.1 (0.1–0.2)	+0.6 (0.3–0.9)	−0.3 (0.2–0.4)	+0.5(0.4–0.6)
Sfc. Pacific/Indian	53 (26–87)	20	5.5	5.5	−6.4 (1.9–13)	−3.0 (2.4–3.5)	+0.5 (0.3–0.8)	+0.3 (0.2–0.4) −0.5(0.2–0.7)	n/a
Intermediate Pacific/Indian	304 (148–496)	1.1	1.7	2.6	−1.1 (0.3–2.2)	+3.0 (2.4–3.5) −1.2 (1.0–1.5)	negligible	−0.2 (0.1–0.4)	+0.2 (0.2–0.3)
Surface Antarctic	16 (10–22)	5.0	2.8	2.5	−0.06 (0.02–0.11)	−0.02 (0.02–0.03)	+0.001 (0.0–0.001)	+0.5 (0.2–0.7) −0.34 (0.2–0.5)	+0.3 (0.2–0.5) −0.3 (0.2–0.4)
Deep North Atlantic	83 (50–120)	n/a	n/a	n/a	n/a	+0.04 (0.03–0.05) −0.02 (0.02–0.03)	n/a	+0.2 (0.1–0.3) −1.7 (1.1–2.5)	+1.1(0.6–1.9)
Deep Atlantic	225 (115–361)	n/a	n/a	n/a	n/a	+0.7 (0.6–0.9) −0.4 (0.3–0.5)	n/a	+1.7 (1.1–2.5) −1.1 (0.6–1.8)	n/a
Bottom Atlantic	44 (23–69)	n/a	n/a	n/a	n/a	+0.4 (0.3–0.5) −0.4 (0.3–0.5)	n/a	+0.2 (0.1–0.3) −0.2 (0.1–0.3)	n/a
Deep Pacific/Indian	702 (505–923)	n/a	n/a	n/a	n/a	+1.3 (1.1–1.7) −0.7 (0.5–0.8)	n/a	+0.6 (0.4–0.8)	−0.7 (0.6–0.9)
Deep Antarctic	35 (23–48)	n/a	n/a	n/a	n/a	+0.02 (0.02–0.03) −0.01 (0.00–0.01)	n/a	+1.1 (0.6–1.8) −0.8 (0.5–1.1)	+0.3 (0.2–0.4) −0.3 (0.2–0.5)
Deep Mediterranean	7 (5–8)	n/a	n/a	n/a	n/a	+0.09 (0.07–0.11) −0.03 (0.02–0.04)	n/a	−0.05 (0.04–0.06)	+0.06 (0.03–0.09)

[a]Sources of atmospheric deposition are as follows: GC = GEOS-Chem; GH = GRAHM; EM = empirical estimate. Units for contemporary ocean reservoirs are Mmol. Units for fluxes in (+) and out of (−) each compartment are Mmol a^{-1}.

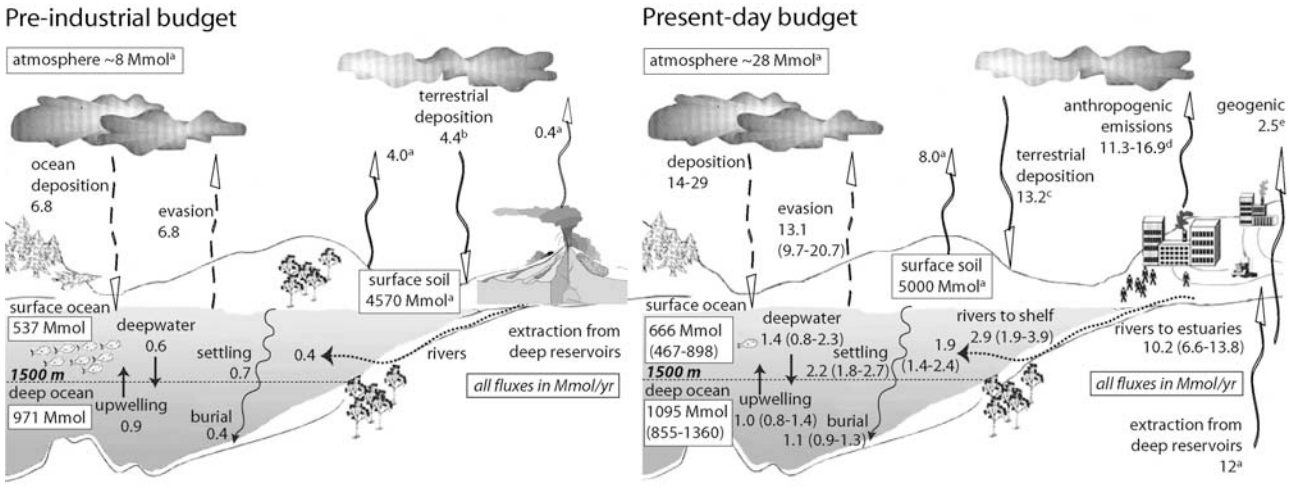

Figure 4. Global budgets for current and preindustrial mercury cycling in oceans. For the present-day ocean, 90% confidence intervals are shown in brackets. Note that for the present-day budget, river fluxes shown refer to the amounts of mercury deposited in each region (estuaries, shelf, open ocean), not the total flux (sum >14 Mmol). (a) From *Mason and Sheu* [2002]. (b) Calculated by assuming preindustrial atmosphere is at steady state. (c) Estimated from sediment core data showing contemporary atmospheric deposition to terrestrial systems is approximately 3 times greater than preindustrial deposition [*Fitzgerald et al.*, 1998]. (d) Lower end of range is year 2000 global anthropogenic emissions from *Pacyna et al.* [2006]. Upper limit of anthropogenic emissions were used in GEOS-Chem simulations and include additional sources described by *Selin et al.* [2007b]. (e) Estimate derived by *Selin et al.* [2007b].

Given the ranges in atmospheric deposition from the three models considered in this study, we calculate an accumulation of 0.2–15 Mmol a^{-1} in the surface 1500 m layer and 1.5 Mmol a^{-1} in the deep ocean. This accumulation is equivalent to 0.03–2% and 0.14% of the estimated contemporary reservoirs of mercury in the surface and deep oceans, respectively, which falls between previously estimated increases in the global atmospheric pool (<2% per annum) and surface soils (~0.17% per annum) [*Mason and Sheu*, 2002].

[34] Our global budget also indicates that total dissolved and particulate phase mercury inputs to coastal and open ocean regions from rivers are large (>14 Mmol a^{-1}) but actual inputs to the open ocean are small (~1.9 Mmol a^{-1}), as shown in other studies [*Cossa et al.*, 1997; *Mason et al.*, 1994a; *Mason and Sheu*, 2002]. We estimate that settling of particle associated mercury in rivers on the shelf and in estuarine regions accounts for a flux of >13 Mmol a^{-1}, which is comparable in magnitude to annual anthropogenic emissions. These large mercury inputs to near-shore marine areas warrant further consideration as a source for methylmercury to fish feeding in these biologically productive regions.

3.3. Anthropogenic Enrichment Since Industrialization

[35] Comparing our contemporary and steady state preindustrial global budgets shows that anthropogenic activities have increased surface and deep ocean mercury reservoirs by ~25% and 11%, respectively (Figure 4). This enrichment is much smaller than the two-to-five-fold estimated increase in the global atmospheric mercury reservoir [*Fitzgerald et al.*, 1998; *Hermanson*, 1993; *Mason et al.*, 1994a]. Running the contemporary ocean model to steady state with present-day atmospheric inputs results in a global-scale increase of 79% in surface waters (up to 1500 m depth) and >150% in the deep ocean (Figure 5). Our modeling shows that there is a significant lag between changes in atmospheric deposition and open ocean mercury concentrations. Results suggest that on average mercury concentrations will continue to increase globally if anthropogenic emissions remain at present levels.

[36] These global enrichment estimates understate regional-scale anthropogenic impacts. Modeled anthropogenic enrichment of the contemporary ocean is greater than 50% in the surface waters of the Atlantic (35°S–55°N), North Atlantic (>55°N), Pacific/Indian (40°S–30°N), and Mediterranean Sea, and the deep North Atlantic (>55°N) (Table 4). In contrast, our modeling results show that intermediate and deep waters of the Pacific/Indian oceans have so far been relatively unaffected (<1%–5% enrichment) by anthropogenic mercury releases (Table 4).

[37] Basin-wide trends in mercury concentrations observed here are generally consistent with regional variability in historical anthropogenic emissions. Over the past several hundred years, anthropogenic emissions are thought to have been largely concentrated in industrial regions of Europe and North America that are adjacent to the Atlantic Ocean and Mediterranean Sea [*Pirrone et al.*, 1996, 1998]. Emissions in these regions have declined considerably in recent decades because of increasing regulatory controls, phase-

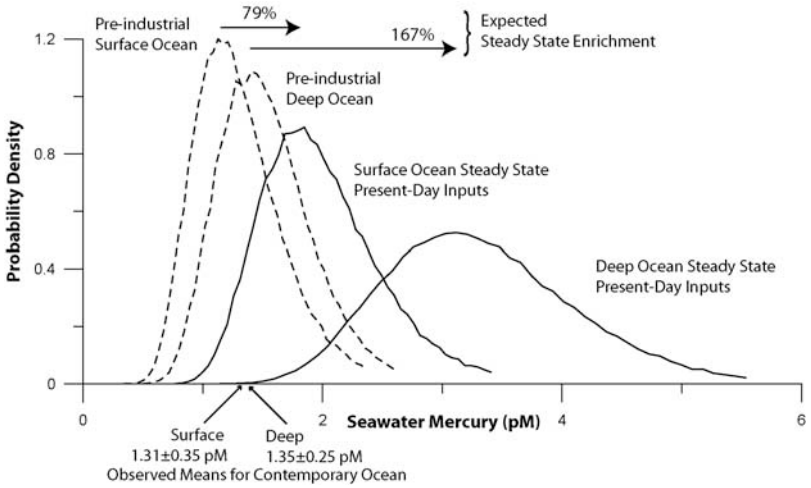

Figure 5. Modeled mercury concentrations in the preindustrial and steady state surface and deep oceans. Expected enrichment of the surface and deep ocean at steady state is calculated as the summed product of probabilities and magnitudes of different seawater concentrations modeled using 100 000 Monte Carlo trials.

outs of products containing mercury, and technological advances [*Pacyna et al.*, 2006; *Pacyna and Pacyna*, 2002; *Pacyna*, 1984]. In contrast, sources of mercury emissions in Asian countries and India that are adjacent to much of the Pacific Ocean have increased relatively recently with rising demand for coal-fired electricity and abundant small-scale gold mining [*Pacyna et al.*, 2006; *Pirrone et al.*, 1996; *Seigneur et al.*, 2004]. Accordingly, our modeling shows that surface waters of much of the Atlantic Ocean and deep water in North Atlantic contain a large signal of historically deposited anthropogenic mercury that is slowly circulating throughout the other ocean basins (Table 4 and Figure 4). Recent trends in emissions also help to explain predicted net losses of mercury to the atmosphere in the Atlantic and Mediterranean compared to net uptake in the Pacific/Indian oceans (Table 3).

3.4. Temporal Responses

[38] Figure 6 shows the near-term trajectory of seawater mercury concentrations in many basins differs depending on the atmospheric model used to derive deposition (GEOS-Chem, GRAHM, empirical best estimate). As discussed above, the magnitude of atmospheric inputs to surface oceans is one of the largest uncertainties in our model.

Table 4. Modeled Anthropogenic Enrichment and Response Times of Ocean Basins

Region	Present-Day AEF,[a] %	Time to Steady State,[b] years	Steady State,[c] Hg, pM
Surface Ocean	25	n/a	1.7–2.4
North Atlantic (>55°N)	57	50–600	1.9–2.6
Surface Atlantic (35°S–55°N)	58	10–30	1.6–2.6
Intermediate Atlantic (65°S–35°S)	13	500–800	2.6–3.4
Surface Med. (30°N–35°N)	68	10–50	1.9–3.3
North Pacific (>30°N)	9	500–700	1.9–3.4
Surface Pacific/Indian (40°S–30°N)	56	10–25	1.3–4.0
Intermediate Pacific/Indian (65°S–40°S)	5	>1000	1.3–1.4
Surface Antarctic (>65°S)	25	800–1000	1.4–2.4
Deep Ocean	11	n/a	2.8–3.6
Deep North Atlantic (>55°N)	63	10–500	2.0–2.7
Deep Atlantic (65°S–55°N)	32	700–1000	2.6–3.5
Bottom Atlantic (65°S–55°N)	7	800–1000	2.1–2.8
Deep Pacific and Indian (<65°S)	<1	>1500	3.0–3.7
Deep Antarctic (>65°S)	4	700–>1000	2.4–3.5
Deep Mediterranean (30°N–35°N)	54	200–300	3.4–5.9

[a]Modeled present-day anthropogenic enhancement factor (AEF) for mercury in seawater.
[b]Estimated response times of different ocean basins to changes in atmospheric deposition calculated by modeling time required to reach steady state (defined as 95% of true steady state) under a variety of atmospheric deposition scenarios.
[c]Ranges of probabilistically modeled seawater Hg at steady state with contemporary atmospheric deposition from three atmospheric models (GEOS-Chem, GRAHM, empirical).

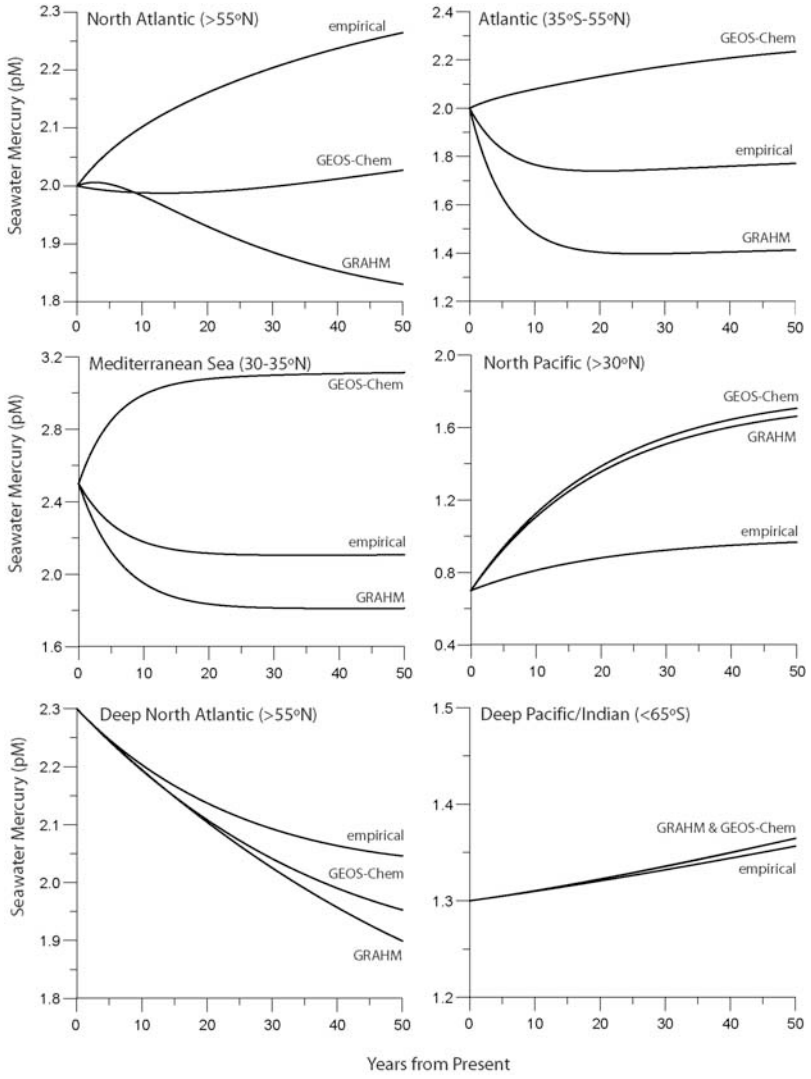

Figure 6. Modeled near-term trajectories of mercury concentrations in selected ocean basins with no change in current atmospheric deposition rates. Scenarios shown illustrate the effects of differences in atmospheric deposition rates from the three atmospheric models used in this study (GRAHM, GEOS-Chem, and empirical best estimate) on seawater mercury concentration trends.

Although there is considerable variability in the trajectory of ocean responses, midrange atmospheric deposition scenarios for each basin indicate that the Atlantic and Mediterranean are likely to decline in mercury if present emissions are held constant (Figure 6). In contrast, the Pacific/Indian oceans and other deeper ocean waters will increase very gradually over time, with the exception of the deep North Atlantic (Figure 6 and Table 4).

[39] These modeled near-term responses are generally consistent with limited data on trends in seawater mercury concentrations over the past several decades. For example, *Laurier et al.* [2004] observed that mercury concentrations in surface waters of the North Pacific have been relatively constant over the past 20 years and that there is little variability in vertical concentration profiles. In contrast, *Gill and Fitzgerald* [1988] and *Mason et al.* [2001] both observed a notable increase in mercury concentrations at the depth of the permanent thermocline in the vicinity of Bermuda that they hypothesized to be a signal from historical anthropogenic emissions. Additionally, overall, concentrations reported by *Mason et al.* [2001] were a factor of 2 lower than the earlier measurements. In addition, *Olafsson* [1983] reported early concentration data from the North Atlantic (11 ± 5 pM) that are much higher than more recent measurements (~2 pM) (Table 2), although this may to some extent be an artifact of improvements in sampling and analytical techniques. Finally, a number of recent studies support the premise that mercury concentrations are declining in the Mediterranean Sea [*Hedgecock et al.*, 2006; *Rajar et al.*, 2007; *Zagar et al.*, 2007].

[40] By running the contemporary ocean model in a time-dependent mode to steady state (defined as the time to reach 95% of the true steady state solution), we obtain information on the relative response times of each ocean basin

Table 5. Sensitivity Analyses Showing Probabilistic Model Parameters With Largest Contributions to Variance in Forecasted Global Surface and Deep Water Concentrations at Steady State Shown in Figure 5[a]

Atmospheric Model Scenario/ Rank	Surface Ocean Variance, %	Deep Ocean Variance, %
Rank 1		
Empirical	$f_{Hg(0)}$ IPI (−18.0)	$f_{Hg(0)}$ SA (−24.1)
GEOS-CHEM	$f_{Hg(0)}$ SPI (−45.8)	$f_{Hg(0)}$SPI (−28.7)
GRAHM	$f_{Hg(0)}$ IPI (−18.0)	$f_{Hg(0)}$ SA (−19.4)
Rank 2		
Empirical	$f_{Hg(0)}$ SPI (−14.4)	C_w DPI (11.9) $f_{Hg(0)}$
GEOS-CHEM	$f_{Hg(0)}$ SA (−13.7)	SA (−21.2) $f_{Hg(0)}$
GRAHM	$f_{Hg(0)}$ SA (−15.9)	DPI (13.5)
Rank 3		
Empirical	$f_{Hg(0)}$ IPI (−13.8)	$f_{Hg(0)}$ IPI (−8.2)
GEOS-CHEM	C_w SPI (−6.5)	C_w DPI (8.1)
GRAHM	$f_{Hg(0)}$ SPI (−15.8)	$f_{Hg(0)}$ IPI (−11.0)
Rank 4		
Empirical	C_w IA (13.8)	$f_{Hg(0)}$ SPI (−7.5)
GEOS-CHEM	C_w IA (6.1)	C_w SPI (−6.3)
GRAHM	C_w IPI (14.5)	C_w IPI (−8.4)
Rank 5		
Empirical	C_w IPI (11.5)	C_w IA (−6.2)
GEOS-CHEM	$f_{Hg(0)}$ IPI (−5.6)	$f_{Hg(0)}$ IPI (−4.4)
GRAHM	C_w IA (10.5)	$f_{Hg(0)}$ SPI (−8.1)

[a]The $f_{Hg(0)}$ is the distribution representing the fraction of dissolved Hg(0) in surface waters on the basis of values reported in Table 1, and C_w is the distribution for contemporary mercury concentrations in each basin. Model compartments shown in Figure 1 are denoted: DPI = Deep Pacific and Indian; IA = Intermediate Atlantic; IPI = Intermediate Pacific/Indian; SA = Surface Atlantic; and SPI = Surface Pacific and Indian.

(Table 4). Our results show that relatively shallow (300 m) mixed layers in the Atlantic and Mediterranean will respond to changes in loading much more rapidly (on the order of decades) than intermediate and deep waters of the Pacific/Indian oceans (>1000 years). These results also help to explain variability in anthropogenic enrichment of mercury among different ocean basins (Table 4).

4. Conclusion

[41] The modeling presented here shows that, in addition to atmospheric deposition, regional-scale variability in air-sea exchange of mercury, particulate settling, and lateral and vertical seawater flow are all important for determining the direction and rate of change of mercury concentrations in the open ocean. Differences among physical and biological properties of ocean basins help to explain why modeled anthropogenic enrichment of mercury varies from <1% in the deep waters of the Pacific/Indian oceans to >60% in the Mediterranean and North Atlantic. Wide ranges in confidence intervals (Table 3 and Figure 3) for many model results reflect uncertainty in model parameters due to data limitations and natural stochasticity in mercury concentrations among geographic regions. In particular, sensitivity analyses indicate that variability in the observed fraction of dissolved Hg(0) in the water column in the surface waters accounts for the majority (48–66%) of the variance in probabilistically modeled seawater concentrations (Figure 5 and Table 5). These results reinforce the importance of collecting additional monitoring data to better constrain air-sea exchange estimates for mercury.

[42] Global mass budgets presented here show surface and deep ocean mercury reservoirs have increased by ~25% and ~11%, respectively, mainly because of anthropogenic enrichment of atmospheric mercury deposition (Figure 5). In addition, mass budgets show that the contemporary ocean is not at steady state with atmospheric inputs and will continue to increase, on average, if present-day emissions remain constant. If the ocean were to reach steady state with present-day atmospheric inputs, anthropogenic mercury enrichment would increase substantially to ~80% in the surface ocean and >150% in the deep ocean. However, most basins will experience a considerable delay between changes in atmospheric inputs and seawater concentrations. Modeled temporal lags of different basins range from decades in the surface waters of the Atlantic to many centuries in the Pacific/Indian oceans. These results help to explain why mercury concentrations may now be declining in the parts of the Atlantic Ocean and Mediterranean but are likely to increase in the North Pacific and Pacific oceans (Figure 6) in a manner consistent with recent geographic trends anthropogenic mercury releases.

[43] Finally, we show that inputs of mercury from rivers to shelf and estuarine regions are >13 Mmol a^{-1} and are comparable in magnitude to direct annual anthropogenic emissions of mercury. Hence bioavailability of mercury discharged from rivers to near-shore marine areas deserves further consideration as a substrate for methylmercury production and potential uptake by estuarine and marine fish.

[44] **Acknowledgments.** Views expressed in this manuscript reflect the authors' professional views and opinions and should not be construed to represent any determination or policy of the U.S. Environmental Protection Agency. We thank Noelle Selin and Daniel Jacob at Harvard University for useful discussion related to this manuscript and GEOS-Chem model results. We also thank Ashu Dastoor and Didier Davignon at Environment Canada for providing GRAHM model results and Chris Knightes at the U.S. EPA for review of several versions of this manuscript.

References

Andersson, M. E., K. Gardfeldt, I. Wangberg, F. Sprovieri, N. Pirrone, and O. Lindqvist (2007), Seasonal and daily variation of mercury evasion at coastal and off shore sites from the Mediterranean Sea, *Mar. Chem.*, *104*, 214–226.

Antia, A. N., et al. (2001), Basin-wide particulate carbon flux in the Atlantic Ocean: Regional export patterns and potential for CO_2 sequestration, *Global Biogeochem. Cycles*, *15*(4), 845–862.

Antoine, D., J.-M. Andre, and A. Morel (1996), Ocean primary production: 2. Estimation at global scale from satellite (coastal zone color scanner) chlorophyll, *Global Biogeochem. Cycles*, *10*(1), 57–69.

Champoux, L., D. C. Masse, D. Evers, O. P. Lane, M. Plante, and S. T. A. Timmermans (2006), Assessment of mercury exposure and potential effects on common loons (Gavia immer) in Quebec, *Hydrobiologia*, *567*, 263–274.

Chester, R. (2003), The transport of material to the oceans: Relative flux magnitudes, in *Marine Geochemistry*, edited by R. Chester, pp. 98–106, Blackwell Sci., Oxford, UK.

Choe, K.-Y., G. A. Gill, and R. Lehman (2003), Distribution of particulate, colloidal, and dissolved mercury in San Francisco Bay estuary: 1. Total mercury, *Limnol. Oceanogr.*, *48*(4), 1535–1546.

Clarkson, T. W., and L. Magos (2006), The toxicology of mercury and its chemical compounds, *Critical Rev. Toxicol.*, *36*(8), 609–662.

Coquery, M., D. Cossa, and J. M. Martin (1995), The distribution of dissolved and particulate mercury in 3 Siberian estuaries and adjacent Arctic coastal waters, *Water Air Soil Pollut.*, *80*, 653–664.

Cossa, D., J. M. Martin, K. Takayanagi, and J. Sanjuan (1997), The distribution and cycling of mercury species in the western Mediterranean, *Deep Sea Res., Part II*, *44*(3–4), 721–740.

Cossa, D., M. H. Cotte-Krief, R. P. Mason, and J. Bretaudeau-Sanjuan (2004), Total mercury in the water column near the shelf edge of the European continental margin, *Mar. Chem.*, *90*, 21–29.

Dai, A., and K. E. Trenberth (2002), Estimates of freshwater discharge from continents: Latitudinal and seasonal variations, *J. Hydrometeorol.*, *3*(6), 660–687.

Dalziel, J. A. (1995), Reactive mercury in the eastern North Atlantic and southeast Atlantic, *Mar. Chem.*, *49*, 307–314.

Dastoor, A. P., and Y. Larocque (2004), Global circulation of atmospheric mercury: A modeling study, *Atmos. Environ.*, *38*, 147–161.

Ferrara, R., C. Ceccarini, E. Lanzillotta, K. Gardfeldt, J. Sommar, M. Horvat, M. Logar, V. Fajon, and J. Kotnik (2003), Profiles of dissolved gaseous mercury concentration in the Mediterranean seawater, *Atmos. Environ.*, suppl. 1, S85–S92.

Fitzgerald, W. F., D. R. Engstrom, R. P. Mason, and E. A. Nater (1998), The case for atmospheric mercury contamination in remote areas, *Environ. Sci. Technol.*, *32*, 1–7.

Gardfeldt, K., et al. (2003), Evasion of mercury from coastal and open waters of the Atlantic Ocean and the Mediterranean Sea, *Atmos. Environ.*, suppl. 1, S73–S84.

Gill, G. A., and W. F. Fitzgerald (1988), Vertical mercury distributions in the oceans, *Geochim. Cosmochim. Acta*, *52*, 1719–1728.

Han, F., X. Q. Shan, S. Z. Zhang, and B. Wen (2004), Mercury speciation in China's coastal surface seawaters, *Int. J. Environ. Anal. Chem.*, *84*(8), 583–598.

Hedgecock, I. M., and N. Pirrone (2004), Chasing quicksilver: Modeling the atmospheric lifetime of Hgo (g) in the marine boundary layer at various latitudes, *Environ. Sci. Technol.*, *38*, 69–75.

Hedgecock, I. M., N. Pirrone, G. A. Trunfio, and F. Sprovieri (2006), Integrated mercury cycling, transport, and air-water exchange (MECAWEx) model, *J. Geophys. Res.*, *111*, D20302, doi:10.1029/2006JD007117.

Hermanson, M. H. (1993), Historical accumulation of atmospherically derived pollutant trace metals in the arctic as measured in dated sediment cores, *Water Sci. Technol.*, *28*(8–9), 33–41.

Horvat, M., M. Logar, J. Kotnik, V. Fajon, T. Zvonaric, and N. Pirrone (2003), Speciation of mercury in surface and deep-sea waters in the Mediterranean Sea, *Atmos. Environ.*, *37*, S93–S108, suppl. 1.

Howard, M. T., A. M.E. Winguth, C. Klaas, and E. Maier-Reimer (2006), Sensitivity of ocean carbon tracer distributions to particulate organic flux parameterizations, *Global Biogeochem. Cycles*, *20*, GB3011, doi:10.1029/2005GB002499.

Jahnke, R. A. (1996), The global ocean flux of particulate organic carbon: Areal distribution and magnitude, *Global Biogeochem. Cycles*, *10*(1), 71–88.

Kahana, R., G. R. Bigg, and M. R. Wadley (2004), Global ocean circulation modes derived from a multiple box model, *J. Phys. Oceanogr.*, *34*, 1811–1823.

Kim, J. P., and W. F. Fitzgerald (1986), Sea-air partitioning of mercury in the equatorial Pacific Ocean, *Science*, *231*(4742), 1131–1133.

Lamborg, C. H., K. R. Rolfhus, and W. F. Fitzgerald (1999), The atmospheric cycling and air-sea exchange of mercury species in the south and equatorial Atlantic Ocean, *Deep Sea Res., Part II*, *46*, 957–977.

Lamborg, C. H., W. F. Fitzgerald, J. O'Donnell, and T. Torgersen (2002), A non-steady state compartmental model of global-scale mercury biogeochemistry with interhemispheric atmospheric gradients, *Geochim. Cosmochim. Acta*, *66*, 1105–1118.

Lamborg, C. H., K. L. Von Damm, W. F. Fitzgerald, C. R. Hammerschmidt, and R. Zierenberg (2006), Mercury and monomethylmercury in fluids from Sea Cliff submarine hydrothermal field, Gorda Ridge, *Geophys. Res. Lett.*, *33*, L17606, doi:10.1029/2006GL026321.

Laurier, F. J. G., R. P. Mason, L. Whalin, and S. Kato (2003), Reactive gaseous mercury formation in the North Pacific Ocean's marine boundary layer: A potential role of halogen chemistry, *J. Geophys. Res.*, *108*(D17), 4529, doi:10.1029/2003JD003625.

Laurier, F. J. G., R. P. Mason, G. A. Gill, and L. Whalin (2004), Mercury distributions in the North Pacific Ocean: 20 years of observations, *Mar. Chem.*, *90*, 3–19.

Laws, E. A., P. G. Falkowski, W. O. Smith Jr., H. Ducklow, and J. J. McCarthy (2000), Temperature effects on export production in the open ocean, *Global Biogeochem. Cycles*, *14*(4), 1231–1246.

Liss, P. S., and P. G. Slater (1974), Flux of gases across the air-sea interface, *Nature*, *247*, 181–184.

Ludwig, W., J. L. Probst, and S. Kempe (1996), Predicting oceanic input of organic carbon by continental erosion, *Global Biogeochem. Cycles*, *10*(1), 23–41.

Mason, R. P., and W. F. Fitzgerald (1991), Mercury speciation in open ocean waters, *Water Air Soil Pollut.*, *56*, 779–789.

Mason, R. P., and W. F. Fitzgerald (1993), The distribution and biogeochemical cycling of mercury in the equatorial Pacific Ocean, *Deep Sea Res.*, *40*, 1897–1924.

Mason, R. P., and G. A. Gill (2005), Mercury in the marine environment, in *Mercury: Sources, Measurements, Cycles and Effects*, edited by M. B. Parsons and J. B. Percival, pp. 179–216, *Short Course Ser.*, vol. 34, Mineral. Assoc. of Canada, Halifax, Nova Scotia, Canada.

Mason, R. P., and G.-R. Sheu (2002), Role of the ocean in the global mercury cycle, *Global Biogeochem. Cycles*, *26*(4), 1093, doi:10.1029/2001GB001440.

Mason, R. P., and K. A. Sullivan (1999), The distribution and speciation of mercury in the south and equatorial Atlantic, *Deep Sea Res., Part II*, *46*, 937–956.

Mason, R. P., W. F. Fitzgerald, and F. M. M. Morel (1994a), The biogeochemical cycling of elemental mercury: Anthropogenic influences, *Geochim. Cosmochim. Acta*, *58*, 3191–3198.

Mason, R. P., J. O'Donnell, and W. F. Fitzgerald (1994b), Elemental mercury cycling within the mixed layer of the equatorial Pacific Ocean, in *Mercury Pollution: Integration and Synthesis,* edited by C. J. Watras and J. W. Huckabee, pp. 83–97, Lewis Publ., Boca Raton, Fla.

Mason, R. P., K. R. Rolfhus, and W. F. Fitzgerald (1995a), Methylated and elemental mercury cycling in surface and deep-ocean waters of the North Atlantic, *Water Air Soil Pollut.*, *80*, 665–677.

Mason, R. P., F. M. M. Morel, and H. F. Hemond (1995b), The role of microorganisms in elemental mercury formation in natural-waters, *Water Air Soil Pollut.*, *80*, 775–787.

Mason, R. P., K. R. Rolfhus, and W. F. Fitzgerald (1998a), Mercury in the North Atlantic, *Mar. Chem.*, *61*, 37–53.

Mason, R. P., N. Bloom, S. Cappellino, G. Gill, J. Benoit, and C. Dobbs (1998b), Investigation of porewater sampling method for mercury and methylmercury, *Environ. Sci. Technol.*, *32*, 4031–4040.

Mason, R. P., N. M. Lawson, and G.-R. Sheu (2001), Mercury in the Atlantic Ocean: Factors controlling air-sea exchange of mercury and its distribution in the upper waters, *Deep Sea Res., Part II*, *48*, 2829–2853.

Maurice-Bourgoin, L., B. Quemerais, P. Moreira-Tureq, and P. Seyler (2003), Transport, distribution and speciation of mercury in the Amazon River at the confluence of black and white waters of the Negro and Solimoes Rivers, *Hydrol. Process.*, *17*, 1405–1417.

Nightingale, P. D., G. Malin, C. S. Law, A. J. Watson, P. S. Liss, M. I. Liddicoat, J. Boutin, and C. Upstill-Goddard (2000), In situ evaluation of air-sea gas exchange parameterizations using novel conservative and volatile tracers, *Global Biogeochem. Cycles*, *14*(1), 373–387.

Olafsson, J. (1983), Mercury concentrations in North Atlantic in relation to cadmium, aluminum, and oceanographic parameters, in *Trace Metals in Sea Water*, *NATO Sci. Ser. IV*, vol. 9, edited by C. S. Wong et al., pp. 475–486, Plenum, New York.

Pace, M., G. A. Knauer, D. M. Karl, and J. H. Martin (1987), Primary production, new production and vertical flux in the eastern Pacific, *Nature*, *325*, 803–804.

Pacyna, E. G., and J. M. Pacyna (2002), Global emissions of anthropogenic mercury sources in 1995, *Water Air Soil Pollut.*, *137*, 149–165.

Pacyna, E. G., J. M. Pacyna, F. Steenhuisen, and S. Wilson (2006), Global anthropogenic mercury emission inventory for 2000, *Atmos. Environ.*, *40*, 4048–4063.

Pacyna, J. M. (1984), Estimation of atmospheric emissions of trace elements from anthropogenic sources in Europe, *Atmos. Environ.*, *18*, 41–50.

Pirrone, N., G. J. Keeler, and J. O. Nriagu (1996), Regional differences in worldwide emissions of mercury to the atmosphere, *Atmos. Environ.*, *30*, 2981–2987.

Pirrone, N., I. Allegrini, G. J. Keeler, J. O. Nriagu, R. Rossman, and J. A. Robbins (1998), Historical atmospheric mercury emissions and depositions in North America compared to mercury accumulations in sedimentary records, *Atmos. Environ.*, *32*, 929–940.

Quemerais, B., D. Cossa, B. Rondeau, T. T. Pham, P. Gagnon, and B. Fortin (1999), Sources and fluxes of mercury in the St. Lawrence River, *Environ. Sci. Technol.*, *33*(6), 840–849.

Rajar, R., M. Cetina, M. Horvat, and D. Zagar (2007), Mass balance of mercury in the Mediterranean Sea, *Mar. Chem.*, *107*(1), 89–102, doi:10.1016/j.marchem.2006.10.001.

Rice, G., and J. K. Hammitt (2005), Economic valuation of human health benefits of controlling mercury emissions from U. S. coal-fired power plants, report, 243 pp., Northeast States for Coord. Air Use Manage., Boston, Mass.

Seigneur, C., K. Vijayaraghavan, K. Lohman, P. Karamchandani, and C. Scott (2004), Global source attribution for mercury deposition in the United States, *Environ. Sci. Technol.*, *38*, 555–569.

Selin, N. E., D. J. Jacob, R. J. Park, R. M. Yantosca, S. Strode, L. Jaegle, and D. Jaffe (2007a), Chemical cycling and deposition of atmospheric mercury: Global constraints from observations, *J. Geophys. Res.*, *112*, D02308, doi:10.1029/2006JD007450.

Selin, N. E., D. J. Jacob, R. M. Yantosca, S. Strode, L. Jaegle, and E. M. Sunderland (2007b), Global 3-D land-ocean-atmosphere model for mercury. Present-day versus preindustrial cycles and anthropogenic enhancement factors for deposition, *Global Biogeochem. Cycles*, doi:10.1029/2007GB003040, in press.

Slemr, F., E.-G. Brunke, R. Ebinghaus, C. Temme, J. Munthe, I. Wangberg, W. Schroeder, A. Steffen, and T. Berg (2003), Worldwide trends in atmospheric mercury since 1977, *Geophys. Res. Lett.*, *30*(10), 1516, doi:10.1029/2003GL016954.

Stommel, H. M. (1961), Thermohaline convection with two stable regimes of flow, *Tellus*, *13*, 224–230.

Strode, S. A., L. Jaegle, N. E. Selin, D. J. Jacob, R. J. Park, R. M. Yantosca, R. P. Mason, and F. Slemr (2007), Air-sea exchange in the global mercury cycle, *Global Biogeochem. Cycles*, *21*, GB1017, doi:10.1029/2006GB002766.

Subramanian, V., N. Madhavan, R. Saxena, and L. C. Lundin (2003), Nature and distribution of mercury in the sediments of the River Yamuna (tributary of the Ganges), *India, J. Environ. Monit.*, *5*(3), 427–434.

Sunderland, E. M. (2007), Mercury exposure from domestic and imported estuarine and marine fish in the United States seafood market, *Environ. Health Perspect.*, *115*(2), 235–242.

Tariq, J., M. Ashraf, M. Jaffar, and M. Afzal (1996), Pollution status of the Indus River, Pakistan, through heavy metal and macronutrient contents of fish, sediment and water, *Water Res.*, *30*(6), 1337–1344.

Temme, C., F. Slemr, R. Ebinghaus, and J. W. Einax (2003), Distribution of mercury over the Atlantic Ocean in 1996 and 1999–2001, *Atmos. Environ.*, *37*, 1889–1897.

Tomczak, M., and J. S. Godfrey (1994), *Regional Oceanography: An Introduction*, 1st ed., 422 pp., Pergamon, New York.

Trasande, L., P. L. Landrigan, and C. Schechter (2005), Public health and economic consequences of methyl mercury toxicity to the developing brain, *Environ. Health Perspect.*, *113*(5), 590–596.

Wilson, S. J., F. Steenhuisen, J. M. Pacyna, and E. G. Pacyna (2006), Mapping the spatial distribution of global anthropogenic mercury atmospheric emission inventories, *Atmos. Environ.*, *40*, 4621–4632.

Woitke, P., J. Wellmitz, D. Helm, P. Kube, P. Lepom, and P. Litheraty (2003), Analysis and assessment of heavy metal pollution in suspended solids and sediments of the river Danube, *Chemosphere*, *51*, 633–642.

Zagar, D., G. Petkovsek, R. Rajar, N. Sirnik, M. Horvat, A. Voudouri, G. Kallos, and M. Cetina (2007), Modelling of mercury transport and transformations in thee water compartment of the Mediterranean Sea, *Mar. Chem.*, *107*(1), 64–88, doi:10.1016./j.marchem.2007.02.007.

R. P. Mason, University of Connecticut, Department of Marine Sciences, 1080 Shennecossett Road, Groton, CT 06340, USA.

E. M. Sunderland, U.S. EPA Region 1, 1 Congress Street, Suite 1100, Mail Code CWQ, Boston, MA 02114, USA. (sunderland.elsie@epa.gov)